# Improved Detection of a Circular target on Random Rough Surface

Sermsak Jaruwatanadilok, Sumit Roy, and Yasuo Kuga
{sermsak, roy, ykuga}@ee.washington.edu

Dept of EE, University of Washington
Seattle WA, 98195-2500

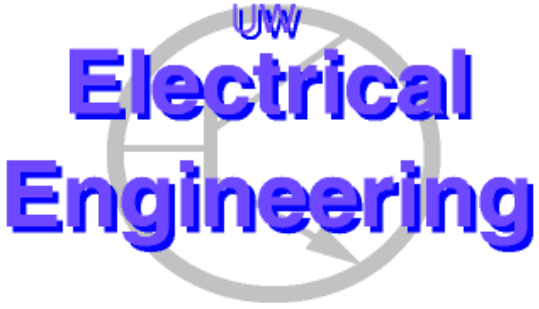


**UWEE Technical Report**
**Number UWEETR-2009-008**
August 18, 2009

Department of Electrical Engineering
University of Washington
Box 352500
Seattle, Washington 98195-2500
PHN: (206) 543-2150
FAX: (206) 543-3842
URL: http://www.ee.washington.edu

# The University of Washington, Department of EE Technical Report Series

Sermsak Jaruwatanadilok, Sumit Roy, and Yasuo Kuga
{sermsak, roy, ykuga}@ee.washington.edu

Dept of EE, University of Washington at Seattle
Seattle WA, 98195-2500

University of Washington, Dept. of EE, UWEETR-2009-008
September 4, 2009

**Abstract**

We consider the problem of detection of a conducting target on a random rough surface and introduce a new method – based on exploiting angular correlation function (ACF) of the backscattered signal to improve detection performance. We show that ACF exhibits better signal to clutter ratio than that of backscatter RCS. We analyze the probability distribution function of the expected returned signal and the correlation function to generate the respective ROC curves and compare performance.

## 1 Introduction

Detection of target in cluttered environment based on electromagnetic wave scattering has been considered for many years [1-3]. In this work, we consider detection of a target situated on top of a random rough surface, whereby the scatter component from the surface is considered to be background clutter. Detector design is traditionally based on the ***difference*** in the characteristics of the returned signal from background clutter alone vis-à-vis target+clutter, and usually only exploits the differences in the observed wave ***intensity*** (or equivalently, radar cross section or RCS) [4],[5]. Our primary contribution is to introduce the use of the angular correlation function (ACF) for enhanced detection which correlates the scattered signal at two different angles. In our previous work, we exploited this strong correlation from rough surface scattering for sea-ice [6] and snow thickness determination [7]. However, in the problem of target detection on random rough surface, the effect from rough surface scattering is to be minimized. The scattered signal from the background as a function of elevation angle exhibits strong peaks at certain combination of frequencies and incident and observed angles. Hence, by careful choice of transmit frequencies and incident and observed angles, we should be able to reduce the effects of rough surface scattering.

## 2 Analytical models for surface correlation functions

Consider the geometry in Fig. 1 (a) consisting of a conducting target of interest against a random rough surface background. A bi-static radar system emits probe signal at an incident angle $\theta_{inc}^{(1)}$, the scattered signal is observed at two angles $\theta_{obs}^{[1]}$ and $\theta_{obs}^{[2]}$. Obvious generalizations include multiple

simultaneous transmitters at respective incident angles $\psi_{inc}^{(2)}$, $\psi_{inc}^{(3)}$, and so on. Fig. 1(b) shows the geometry where there is no target.

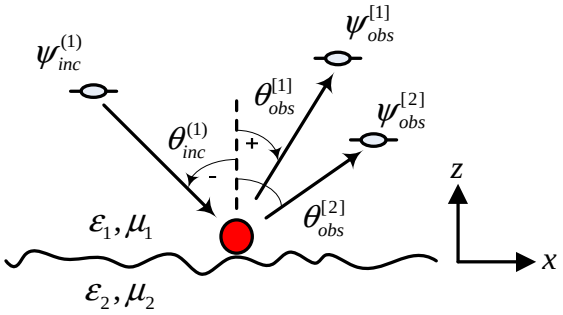


Fig. 1. Geometry of the target detection problem.

First, we limit ourselves to one transmitter and analyze the characteristics of the angular correlation function defined as the statistical expectation of the observed scattered signal at the two elevation angles $\left\langle \psi_{obs}^{[1]}, \psi_{obs}^{[2]*} \right\rangle$. For analytical tractability, we invoke the following assumptions:

(1) Random rough surface has a Gaussian characteristics.
(2) Only first-order perturbation is considered.

In our geometry, the medium 1 is free space ($\varepsilon_1 = \varepsilon_o$; $\mu_1 = \mu_o$) while medium 2 is a lossy dielectric. We define intrinsic propagation constant of the medium 2 by

$$\alpha_2 + j\beta_2 = j\frac{2\pi f}{c}\sqrt{\varepsilon_{r2}} \tag{1}$$

where $\varepsilon_{r2}$ is the complex relative dielectric constant of medium 2. $\alpha_2$ represents a loss constant while $\beta_2$ represents a phase constant. The wave number is given by $k_1 = 2\pi f/c$, $f$ is the frequency of the wave, $c$ is the speed of light. We can see that $\beta_1 = k_1$.The far-field scattered wave is given by [8]

$$\psi_{obs}^{[1]}(K_{obs}, K_{inc}) = \frac{k_1 \cos\theta_{obs}^{[1]}}{\left(2\pi k_1 R^{[1]}\right)^{1/2}} \exp\left(-jk_1 R^{[1]} + j\frac{\pi}{4}\right) S(K_{obs}^{[1]}, K_{inc}^{(1)}) \psi_{inc}^{(1)} \tag{2}$$

where

$$S(K_{obs}^{[1]}, K_{inc}^{(1)}) = \gamma(K_{obs}^{[1]}, K_{inc}^{(1)}) H(K_{obs}^{[1]}, K_{inc}^{(1)})$$

$$S(K_{obs}^{[1]}, K_{inc}^{(1)}) = \gamma(K_{obs}^{[1]}, K_{inc}^{(1)}) H(K_{obs}^{[1]}, K_{inc}^{(1)}),\ \gamma(K_{obs}^{[1]}, K_{inc}^{(1)}) = \frac{1}{2\pi}\frac{jK_{z2}^{(1)} A/\varepsilon_r + B}{jK_{z2}^{(1)}/\varepsilon_r + jK_{inc\_z}^{(1)}},$$

$$\varepsilon_r = \varepsilon_2/\varepsilon_1,\ A = \left(jK_{inc\_z}^{(1)} - jK_{z1}^{(1)}\Gamma - jK_{z2}^{(1)}T\right),\ B = \left(-(K_{inc}^{(1)}K_{obs}^{[1]} - k_1^2)(1+\Gamma) + \frac{1}{\varepsilon_r}(K_{inc}^{(1)}K_{obs}^{[1]} - k_2^2)T\right),$$

$$K_{inc}^{(1)} = \beta_1 \sin\left(\theta_{inc}^{(1)}\right),\ K_{inc\_z}^{(1)} = \beta_1 \cos\left(\theta_{inc}^{(1)}\right),\ K_{z1}^{(1)} = \sqrt{k_1^2 - \left(K_{inc}^{(1)}\right)^2},\ K_{z2}^{(1)} = \sqrt{k_2^2 - \left(K_{inc}^{(1)}\right)^2},$$

$$K_{obs}^{[1]} = \beta_1 \sin\left(\theta_{obs}^{[1]}\right),\ K_{obs}^{[2]} = \beta_1 \sin\left(\theta_{obs}^{[2]}\right)$$

$\Gamma$ is the reflection coefficient, and $T$ is the transmission coefficient. The relationship between $\theta_{obs1}^{[1]}$ and $\theta_{obs2}^{[1]}$ can be found using the Snell's law.

The function $H$ is given by

$$H(K_{obs}^{[1]}, K_{inc}^{(1)}) = \int h(x) \exp\left(-j(K_{obs}^{[1]} - K_{inc}^{(1)})\right) dx \tag{3}$$

where $h(x)$ is the height (relative to a baseline) of the random surface.

The angular correlation function of the observed complex amplitude is given by

$$\left\langle \psi_{obs}^{[1]}(K_{obs}^{[1]}, K_{inc}^{(1)}) \psi_{obs}^{[2]*}(K_{obs}^{[2]}, K_{inc}^{(1)}) \right\rangle = \frac{k_1^2 \cos\theta_{obs}^{[1]} \cos\theta_{obs}^{[2]}}{2\pi k_1 \left(R^{[1]} R^{[2]}\right)^{1/2}} \exp\left(-j(k_1 R^{[1]} - k_1 R^{[2]})\right) \gamma(K_{obs}^{[1]}, K_{inc}^{(1)}) \gamma^*(K_{obs}^{[2]}, K_{inc}^{(1)}) \left\langle H(K_{obs}^{[1]}, K_{inc}^{(1)}) H^*(K_{obs}^{[2]}, K_{inc}^{(1)}) \right\rangle \psi_{inc}^{(1)} \psi_{inc}^{(1)*} \tag{4}$$

where

$$\left\langle H(K_{obs}^{[1]}, K_{inc}^{(1)}) H^*(K_{obs}^{[2]}, K_{inc}^{(1)}) \right\rangle = \iint \left\langle h(x_1) h(x_1') \right\rangle \exp\left(-j\left(K_{obs}^{[1]} - K_{inc}^{(1)}\right) x_1\right) \exp\left(+j\left(K_{obs}^{[2]} - K_{inc\,i1}^{(1)}\right) x_1'\right) dx_1 dx_1'$$

For a random rough surface with Gaussian correlation function,

$$\left\langle h(x_1) h(x_1') \right\rangle = \left\langle h^2 \right\rangle \exp\left(-\frac{x_d^2}{l^2}\right) = \sigma_h^2 \exp\left(-\frac{x_d^2}{l^2}\right) \tag{5}$$

If we have a taper function in the Gaussian form $\exp\left(-x^2 / L_{eq}^2\right)$ we have

$$\left\langle H(K_{obs}^{[1]}, K_{inc}^{(1)}) H^*(K_{obs}^{[2]}, K_{inc}^{(1)}) \right\rangle = \sigma_h^2 \int \exp\left(-\frac{x_c^2}{L_{eq}^2}\right) \exp(-jA_d x_c) dx_c \int \exp\left(-\frac{x_d^2}{l^2}\right) \exp\left(-jA_c x_d\right) dx_d = \sigma_h^2 \pi L_{eq} l \exp\left(-\frac{A_c^2 l^2}{4}\right) \exp\left(-\frac{A_d^2 L_{eq}^2}{4}\right) \tag{6}$$

where

$A = K_{obs}^{[1]} - K_{inc}^{(1)}$, $B = K_{obs}^{[2]} - K_{inc}^{(1)}$, $A_c = (A+B)/2$, $A_d = A - B$, $x_c = \left(x_1 + x_1'\right)/2$, $x_d = x_1 - x_1'$ and $l$ = correlation length; $\sigma_h$ = rms height. This formulation shows that the correlation $\left\langle \psi_{obs}^{[1]}(K_{obs}^{[1]}, K_{inc}^{(1)}) \psi_{obs}^{[2]*}(K_{obs}^{[2]}, K_{inc}^{(1)}) \right\rangle$ is strong when a phase matching condition is met, i.e., $A_d = 0$, which means $K_{obs}^{[1]} - K_{inc}^{(1)} = K_{obs}^{[2]} - K_{inc}^{(1)}$. This is called 'memory line' effect [9] and it will be illustrated in the later section.

We employ the RCS definition [10]

$$\text{RCS} = \lim_{R \to \infty} 2\pi R \frac{\left|\psi_{obs}\right|^2}{\left|\psi_{inc}\right|^2} \tag{7}$$

Note from (2), $\psi_{obs}$ in the far-field is a function of $1/\sqrt{R}$ and the RCS thus does not depend on $R$. For our two-dimensional geometry, RCS is the scattering width or the radar cross section per unit length (and has units of length) [10]. For a fair comparison, we employ the ACF definition

$$\text{ACF} = \lim_{R \to \infty} 2\pi R \frac{\left|\left\langle \psi_{obs}^{[1]}(K_{obs}^{[1]}, K_{inc}^{(1)}) \psi_{obs}^{[2]*}(K_{obs}^{[2]}, K_{inc}^{(1)}) \right\rangle\right|}{\left|\psi_{inc}\right|^2} \tag{8}$$

which also has units of length.

## 3 ACF/FCF characteristics

We compare the behaviors of the angular correlation function and the radar cross section. The numerical simulations are performed using two-dimensional finite-difference time-domain (FDTD) method. The geometry of the simulations is illustrated in Fig. 2. Wave scattering is simulated and the observed wave is calculated in the situation where the perfect electric conductor (PEC) target is present and when there is no target. The rough surface interface has a Gaussian correlation function with the rms height of 2.4 cm and correlation length of 12 cm. PEC target has the size of 10 cm, center frequency of incident wave is 1.5 GHz, ground dielectric constant is $3.7+i0.1$. The incident wave is a tapered plane wave with an incident angle of 20 degree. The grid resolution in the simulation is 50 points per wavelength. PML is used to absorb out-going wave and prevent erroneous scattering.

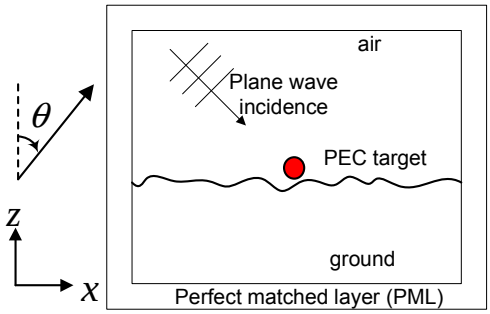


Fig. 2. Geometry of FDTD simulations.

First, we show the memory line characteristics from the analytical derivation. It is confirmed by the FDTD numerical simulation and illustrated in Fig 3. The memory line exhibits strong correlation of scattered wave from rough surface in certain direction. In this case, since we only have one source with a single frequency, the memory line occurs at $\theta_{obs}^{[1]} = \theta_{obs}^{[2]}$. The significance of this memory line is that it is the contribution from rough surface scattering which can be considered unwanted signal in this target detection application. Therefore, in the target detection, observation on this memory line should be avoided.

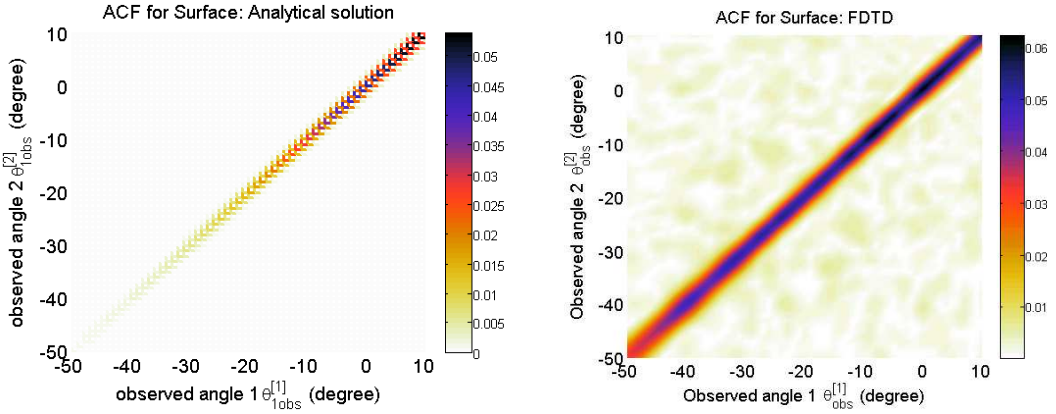


Fig. 3. Memory line for rough surface scattering showing strong correlation at $\theta_{obs}^{[1]} = \theta_{obs}^{[2]}$. Left: analytical solution. Right: FDTD numerical simulation.

Next, we investigate the behavior of the RCS and ACF when target in present compared to the case when it is not present. Plot of ACF and RCS as a function of observation angle is shown in

Fig. 4. However, the evidence of improvement using ACF is better illustrated in Fig. 5 where we compare the signal plus clutter to clutter ratio. Signal plus clutter is the case where the ACF and RCS are calculated when the circular target is present (Fig. 1a) and clutter is the case where the ACF and RCS are calculated when only the random rough surface is present (Fig. 1b). An obvious observation is that the ratio is very small in the specular direction where the strong correlation (memory line) is located. The width of this memory line is inversely proportional to the illumination area $L_{eq}$ in Eq. (6). This illumination area depends on the size of the transmitting antennas and the distance from the transmitting antenna to the ground. Another important observation is that the signal plus clutter to clutter ratio $\left((S+C)/C\right)$ is constantly higher for ACF than RCS, especially when one of the observed angle is fixed at the backscattering direction (ACF configuration 1). ACF configuration 1 also shows almost consistently better $\left((S+C)/C\right)$ than ACF configuration 2. This may be explained by the contribution from random rough surface in the specular direction in ACF configuration 2.

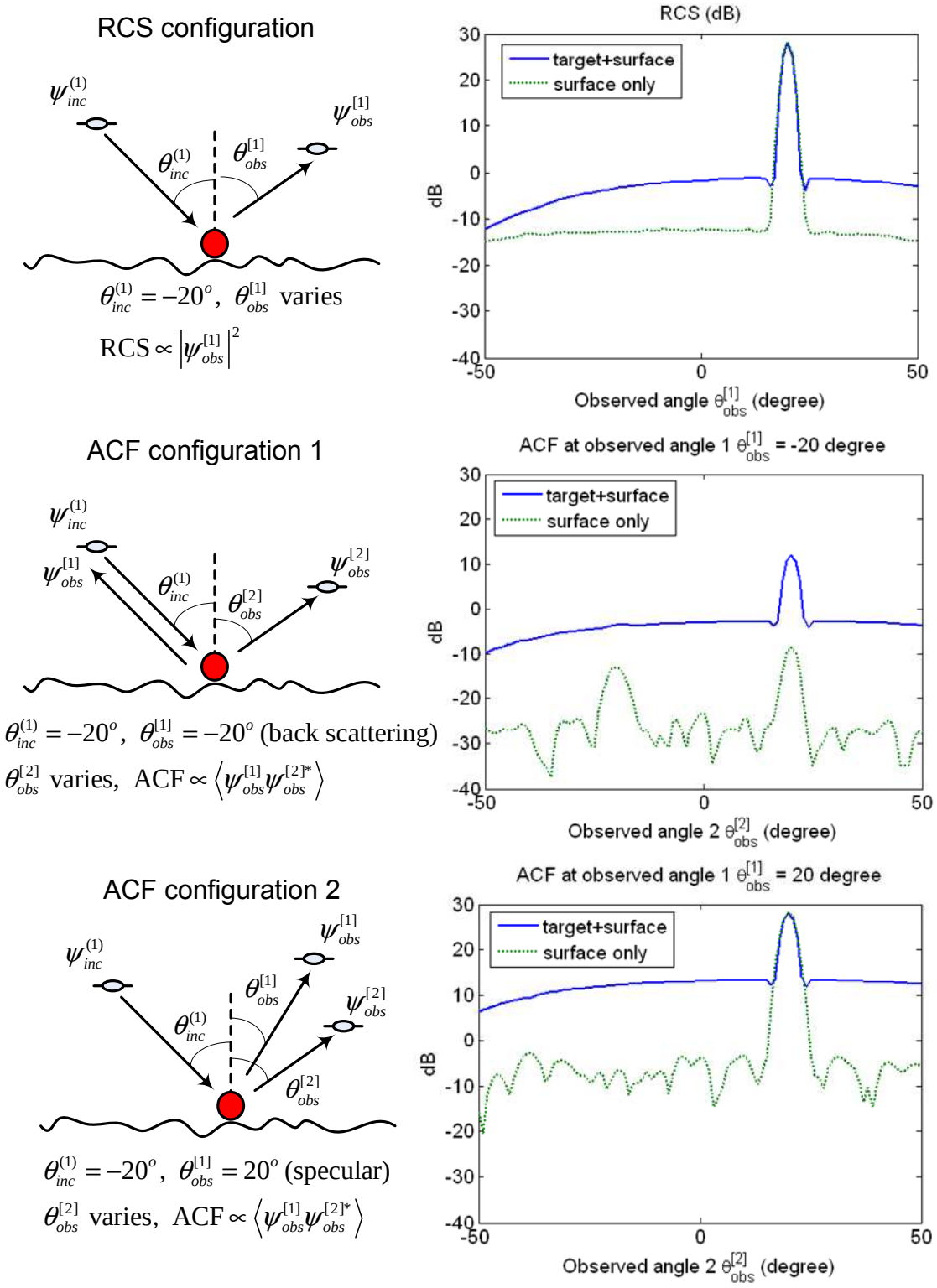


Fig. 4. RCS and ACF configurations and their behaviors as functions of observed angles. The incident angle is fixed at 20 degree.

We further study the case where there is more than one incident wave to see whether we can exploit other correlations or improve detection of the target. The first incident wave has 20 degree incident angle and the second incident wave has 30 degree incident angle. When incident wave comes from two different angles, there exist three distinct strong correlation lines (memory lines) as

shown in Fig. 6. We also calculate the signal plus clutter to clutter ratio in this case. It does not show any significant advantage in improving the signal plus clutter to clutter ratio (Fig. 7).

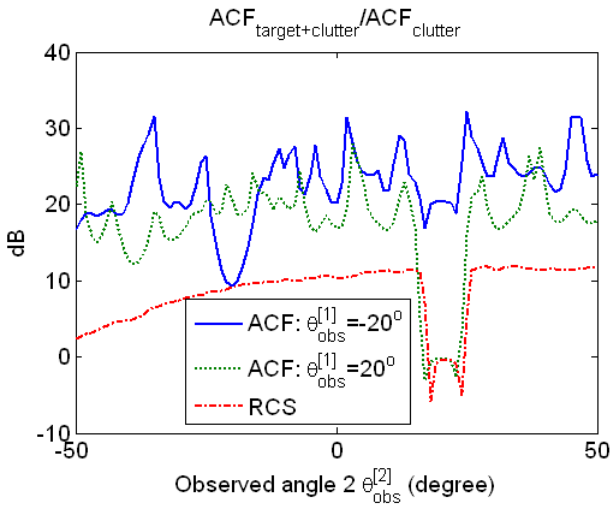


Fig. 5. Signal plus Clutter over Clutter ratio comparison between RCS and two ACF configurations as shown in Fig. 4.

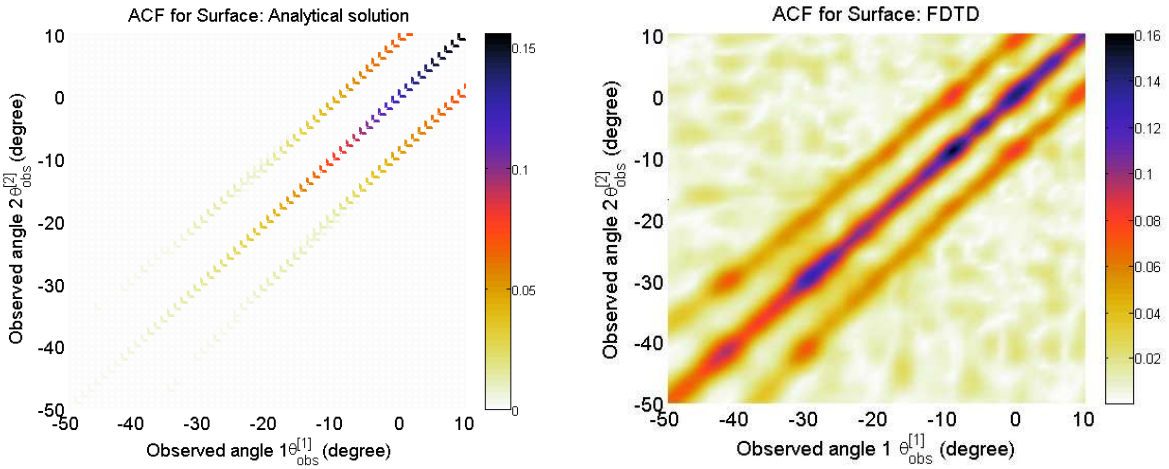


Fig. 6. Memory line for rough surface scattering when there are two incident waves of 20 degree and 30 degree. Top: analytical solution. Bottom: FDTD numerical simulation.

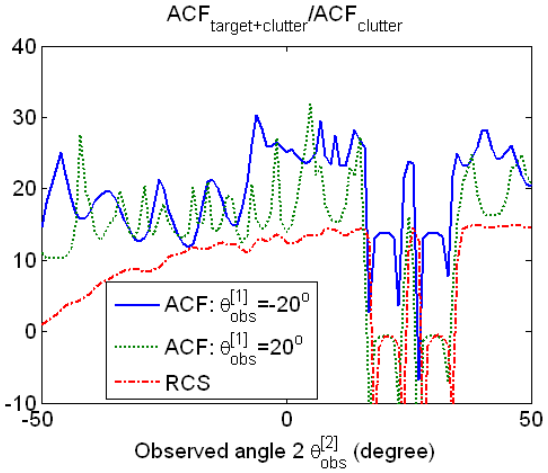


Fig. 7. Signal plus clutter over clutter ratio for two incident wave of 20 degree and 30 degree.

## 4 Probabilistic models of the radar cross section and the angular correlation function

In this section, we investigate the probabilistic models for RCS and ACF of the scattered wave from the random rough surface. The results in this section show the relationship between the rough surface parameters, incident and observed angles to the probabilistic models for RCS and ACF for rough surface scattering. The p.d.f for the rough surface scatter leads to the direct determination of probability of false alarm. Previous investigations into models for intensity or RCS of rough surface backscatter has suggested Weibull-Rician distribution [1],[11], where the parameters of Wiebull-Rician distribution are estimated by fitting to available measurements. On the other hand, analytical solution offers valuable insight into the relationship of physical and system parameters to those in the resulting p.d.f. However, closed form expressions for the latter exist only for specific cases such as random rough surface with Gaussian profiles [12]. The p.d.f. of the ACF of the scattered wave from Gaussian random rough surface has not been derived analytically, to the authors' knowledge, and is done next.

The p.d.f. for the RCS of the Gaussian random surface was derived by [12] and is in the form of an exponential distribution

$$p(u) = \frac{1}{2\sigma_{Rb}^2 \left|K_1\right|^2} \exp\left( -\frac{u}{2\sigma_{Rb}^2 \left|K_1\right|^2} \right); \quad u \geq 0 \tag{9}$$

where the parameter $u$ relates to the RCS by

$$u = RCS \frac{\lambda}{\varepsilon_2 L_{eq}} \tag{10}$$

$$\left|K_1\right| = j2k \cos\theta_{inc}^{(1)} \cos\theta_{obs}^{[1]} \frac{\cos\theta_{obs}^{[1]} - \sqrt{n_2^2 - \sin^2\theta_{obs}^{[1]}}}{\cos\theta_{obs}^{[1]} + \sqrt{n_2^2 - \sin^2\theta_{obs}^{[1]}}}, \sigma_{Rb}^2 = \frac{1}{2}\left[ \hat{S}_{aa}(\xi) + \frac{\sin(\xi L)}{\xi L} \hat{S}_{aa}(0) \right],$$

$$\xi = k\left( \sin\theta_{inc}^{(1)} - \sin\theta_{obs}^{[1]} \right),$$

$\hat{S}_{aa}$ is the power spectrum of the surface. If the autocorrelation function of the surface is Gaussian, we get

$$\hat{S}_{aa}(\gamma) = \frac{\sigma^2 l}{2\sqrt{\pi}} \exp\left( -\frac{\xi^2 l^2}{4} \right)$$

where $l$ =correlation length; $\sigma$ =rms height; $L_{eq}$ = illumination length.

Now, we focus on the p.d.f of the ACF of the scattered wave from a rough surface. From the far-field scattered expression in Eq.(2) and the definition of ACF in Eq.(8). We will derive the p.d.f of the ACF which is defined by $\mathrm{ACF} = \lim_{R\to\infty} \dfrac{2\pi R \left| \psi_{obs}^{[1]}(K_{obs}^{[1]}, K_{inc}^{(1)}) \psi_{obs}^{[2]*}(K_{obs}^{[2]}, K_{inc}^{(1)}) \right|}{\left|\psi_{inc}\right|^2}$.

Let us recall Eq.(2)

$$\begin{aligned} \psi_{obs}^{[1]}(K_{obs}, K_{inc}) &= \frac{k_1 \cos\theta_{obs}^{[1]}}{\left(2\pi k_1 R^{[1]}\right)^{1/2}} \exp\left( -jk_1 R^{[1]} + j\frac{\pi}{4} \right) \gamma_1(K_{obs}^{[1]}, K_{inc}^{(1)}) H(K_{obs}^{[1]}, K_{inc}^{(1)}) \psi_{inc}^{(1)} \\ \psi_{obs}^{[2]}(K_{obs}, K_{inc}) &= \frac{k_1 \cos\theta_{obs}^{[2]}}{\left(2\pi k_1 R^{[2]}\right)^{1/2}} \exp\left( -jk_1 R^{[2]} + j\frac{\pi}{4} \right) \gamma_2(K_{obs}^{[2]}, K_{inc}^{(1)}) H(K_{obs}^{[2]}, K_{inc}^{(1)}) \psi_{inc}^{(1)} \end{aligned} \tag{11}$$

Therefore, using the definition of ACF, we get

$$\begin{aligned}\text{ACF} &= k_1 \cos\theta_{obs}^{[1]} \cos\theta_{obs}^{[2]} \left|\gamma_1(K_{obs}^{[1]}, K_{inc}^{(1)}) H(K_{obs}^{[1]}, K_{inc}^{(1)})\right| \left|\gamma_2(K_{obs}^{[2]}, K_{inc}^{(1)}) H(K_{obs}^{[2]}, K_{inc}^{(1)})\right| \\ &\triangleq k_1 \cos\theta_{obs}^{[1]} \cos\theta_{obs}^{[2]} \left|F_1\right| \left|F_2\right|\end{aligned} \tag{12}$$

Note that function $H(K_{obs}^{[1]}, K_{inc}^{(1)})$ is a random function that is the Fourier transform of the random height $h(x)$ .The functions $F_1 = \gamma_1(K_{obs}^{[1]}, K_{inc}^{(1)}) H(K_{obs}^{[1]}, K_{inc}^{(1)})$ and $F_2 = \gamma_2(K_{obs}^{[2]}, K_{inc}^{(1)}) H(K_{obs}^{[2]}, K_{inc}^{(1)})$ are, in general. If the rough surface height has a Gaussian characteristics, the real and imaginary parts of these functions are also Gaussian distributed since $\gamma_1$ and $\gamma_1$ are both complex constants [12]. By transformation to polar coordinates, the real and imaginary parts are converted to magnitude and phase. With the large illumination area ( $L_{eq} \to \infty$ ), we can assume that the magnitude and phase of functions F's are independent [12]. Thus, we find the p.d.f of the magnitude of the function $F_1$ in the form of Rayleigh distribution as [12]

$$f_{|F_1|}(m) = \frac{m}{\sigma_{R1}^2 |\gamma_1|^2} \exp\left(-\frac{m^2}{2\sigma_{R1}^2 |\gamma_1|^2}\right) \tag{13}$$

where $\sigma_{R1}^2 = \frac{1}{2}\left[\hat{S}_{aa}(\xi_1) + \frac{\sin(\xi_1 L_{eq})}{\xi_1 L_{eq}} \hat{S}_{aa}(0)\right]$, $\xi_1 = k_1\left(\sin\theta_{inc}^{(1)} - \sin\theta_{obs}^{[1]}\right)$, and $\hat{S}_{aa}$ is given in Eq.(10). In other words, the p.d.f of the magnitude of the random scattered field from random rough surface of Gaussian type is in the form of Rayleigh distribution in Eq.(13). The same derivation can be performed for the magnitude of the scattering function $F_2$. The distribution of the magnitude of the function $F_2$ is in the same form as Eq. (13) but the functions $\sigma_{R1}^2$ and $\gamma_1$ become $\sigma_{R2}^2$ and $\gamma_2$ where $\sigma_{R2}^2 = \frac{1}{2}\left[\hat{S}_{aa}(\xi_2) + \frac{\sin(\xi_2 L_{eq})}{\xi_2 L_{eq}} \hat{S}_{aa}(0)\right]$, $\xi_2 = k_1\left(\sin\theta_{inc}^{(1)} - \sin\theta_{obs}^{[2]}\right)$, due to the different angles.

The p.d.f of ACF is therefore the p.d.f of multiplication of two Rayleigh-distributed random variables with two different parameters and a purely real number scaling. With large illumination area ( $L_{eq} \to \infty$ ), we can assume that $F_1$ and $F_2$ are independent, the distribution of the product of two independent Rayleigh random variables. We obtain the p.d.f of $V = \left|F_1\right| \left|F_2\right|$ as the the double-Rayleigh distribution [13],[14], i.e.,

$$f_V(v) = \frac{v}{\sigma_{R1}^2 |\gamma_1|^2 \sigma_{R2}^2 |\gamma_2|^2} K_o\left(\frac{v}{\sigma_{R1}|\gamma_1|\sigma_{R2}|\gamma_2|}\right) \tag{14}$$

where $K_o$ is the modified Bessel function of the second kind and zeroth order. From Eq. (12), the parameter $V$ relates to the ACF by

$$V = \frac{\text{ACF}}{k_1 \cos\theta_{obs}^{[1]} \cos\theta_{obs}^{[2]}} \tag{15}$$

Notice that the ACF of the scattered wave from random rough surface is related to physical parameters including the dielectric constants, the roughness parameters of the surface, and the incident and observed angles. We plot the expression in Eq.(9) and Eq.(14) and compare with the numerical simulations using FDTD method in Fig. 8. In this particular instance, the RCS is calculated for the geometry shown in the top of Fig. 4 where the incident and observation angles equal -20 degree. The ACF is calculated in the case where the incident wave is -20 degree and the observed waves are at -20 degree (backscattering) and at -10 degree. This corresponds to the

geometry shown in the middle of Fig. 4 (ACF configuration 1) where $\theta_{obs}^{[2]} = -10$. The results show that the probabilistic model for RCS (Eq. (10)) and that for the ACF (Eq. (16)) based on Gaussian random rough surface assumptions, matches full wave FDTD numerical simulations. Note that this analytical solution result is derived from the first-order rough surface scattering, which does not include the reflected wave in the specular direction. Therefore, the solution is not valid in the specular direction.

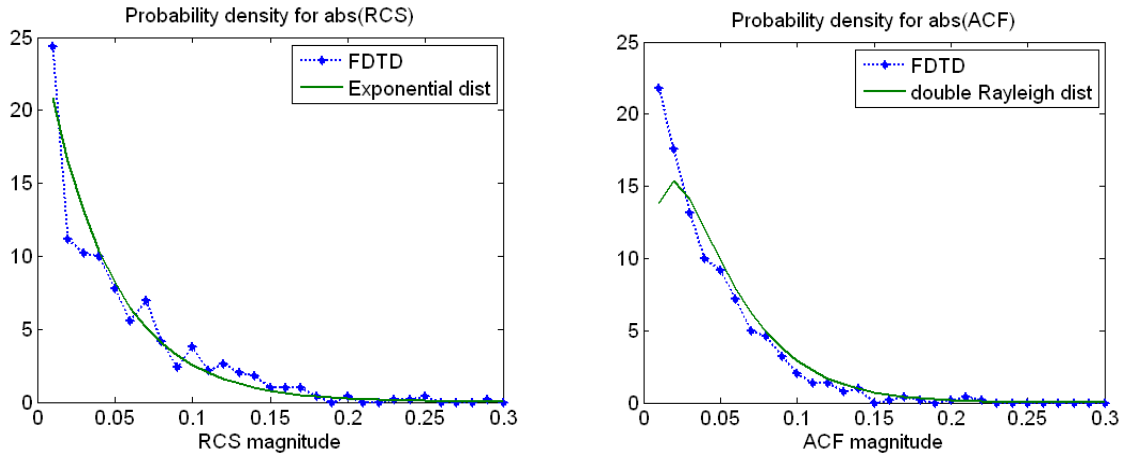


(a) (b)

Fig. 8. The p.d.f of magnitude of RCS and ACF comparison between analytical model and FDTD simulations. (a) Pdf of RCS comparison between Eq. (9) and FDTD. (b) P.d.f of ACF comparison between Eq. (14) and FDTD.

## 5 Target detection performance

### *A. Detection performance comparison between RCS and ACF method*

We apply FDTD method to obtain the probability distribution in the case where there is a target including the RCS and ACF methods. The results are illustrated in Fig. 9. Then, we can calculate the probability of detection versus probability of false alarm of the RCS and ACF method and the result is shown in Fig. 10. This shows that ACF method consistently provides a better probability of detection than RCS method at the same probability of false alarm.

### *B. Change in the observation angles*

Fig. 5 gives the information on which observed angle should be used to form the ACF that will enhance the probability of detection and reduce the probability of false alarm. In the ACF configuration 1 shown in Fig. 4 where the observed wave 1 is the backscattered wave $\theta_{obs}^{[1]} = -20$, we can explore the change in observed angle for the observed wave 2. The followings are the observation from the results shown in Fig. 5 that we can use to pick appropriate observed angles

(1) The signal plus clutter to clutter ratio plotted in Fig. 5 indicates that the ratio for ACF is generally higher than that of RCS. The ratio at $\theta_{obs}^{[2]} = -20$ coincide with the ratio of RCS.

(2) The ratio near the specular direction $\theta_{obs}^{[2]} = 20$ is low because the strong contribution of the memory line. Therefore the observation at or around 20 degree should not be used for correlation calculation.

(3) On the other hand, the wave in the specular direction gives the strong target signal. As a result, when the effect from memory line lessens, the signal plus clutter over clutter ratio can be significant as shown at the observed angle 2 of about 25 degree. The extent of the memory line depends on the illumination distance which directly relates to the size of the antenna used.

We compare the ROC curve for ACF method when the observed angle 2 changes in Fig. 11. This explains the performance of the choices we can make in choosing the observation angles.

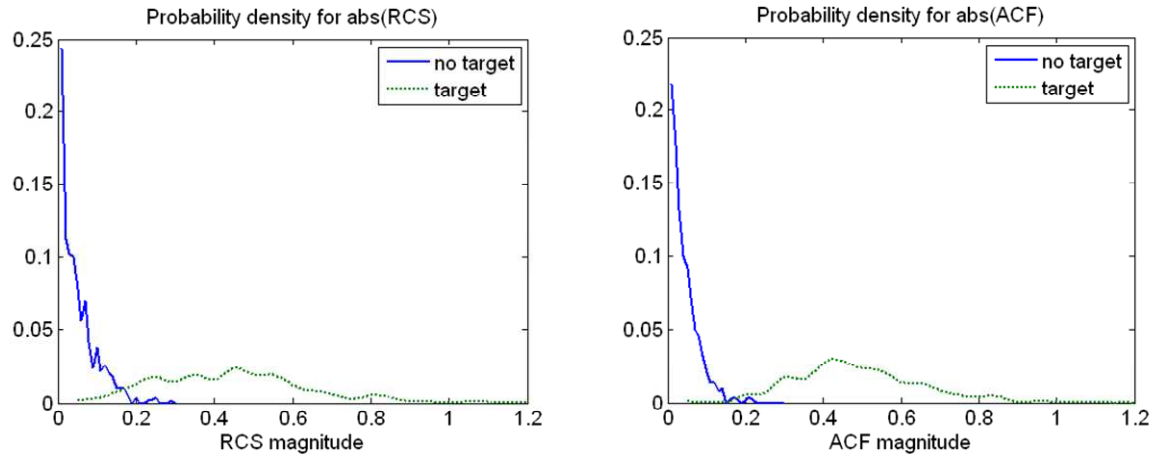


Fig. 9. Probability density of RCS and ACF. In this comparison, the incident wave is 20 degree. RCS is calculated from the backscattering wave with $\theta_{obs}^{[1]} = -20$. ACF is calculated from correlation of the observed wave 1 at backscattering direction $\theta_{obs}^{[1]} = -20$ with the observed wave 2 at $\theta_{obs}^{[2]} = -10$.

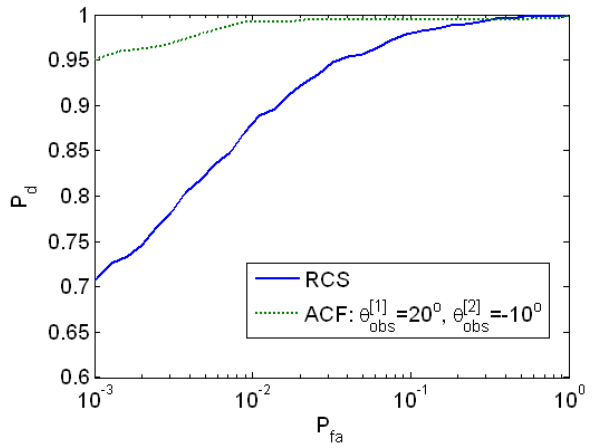


Fig. 10. ROC curve for RCS and ACF calculated from results in Fig. 9.

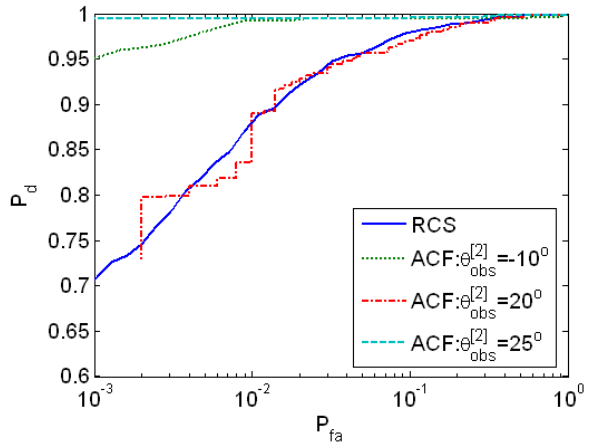


Fig. 11. ROC curve when the incident angle is 20 degree and the observation angle 2 varies showing best performance at the observed angle 2 of 25 degree.

*C. Change in the incident angle*

We now investigate the change in the incident angle to the target detection performance. We perform FDTD numerical simulation when the incident wave is 30 degree. Then, we calculate the signal plus clutter to clutter ratio in the same fashion as we do for the result shown in Fig. 5. It is shown in Fig. 12. We observe similar behaviors as explained in the previous section which leads to the same determination for the observation angles for the best target detection performance. The result of target detection in terms of the probability of detection and probability of false alarm is illustrated in Fig. 13. Comparing to the case where the incident angle is 20 degree, the detection performance when the incident angle is 30 degree deteriorates.

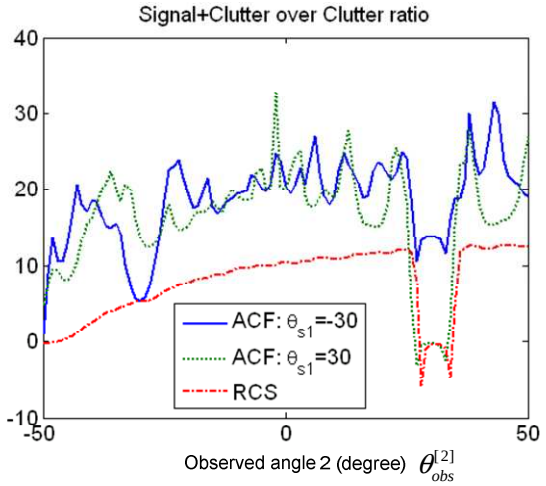


Fig. 12. Signal plus Clutter over Clutter ratio comparison between RCS and two ACF configurations when the incident angle is 30 degree.

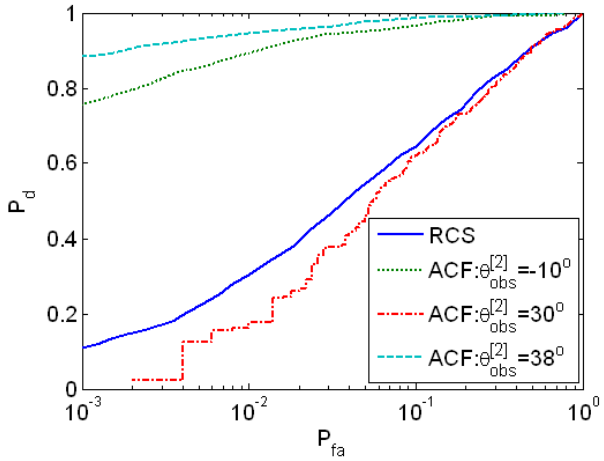


Fig. 13. ROC curve when the incident angle is 30 degree and the observation angle 2 varies showing best performance at the observed angle 2 of 38 degree.

## 6 Conclusions

We consider detection of a conducting circular target on random rough surface. We introduce angular correlation function (ACF) method to improve detection of the target. We show that ACF is superior to the conventional method using radar cross section (RCS) in improving signal plus clutter to clutter ratio. We also analyze the probability density of the ACF and RCS and produce a ROC curve showing the ACF exhibits better performance in the probability of detection vs.

probability of false alarm. We also show the effect of the observation angles to the detection performance and the strategy for choosing appropriate observation angles for the best detection.

**References**


[1] D. C. Schleher, "Radar detection in Weibull clutter," *IEEE Transactions on Aerospace and Electronic Systems*, vol. AES-12, no. 6, pp. 736-743, 1976.

[2] M. Hurtado and A. Nehorai, "Polarimetric detection of targets in heavy inhomogeneous clutter," IEEE *Transactions on Signal Processing*, vol. 56, no. 4, pp. 1349-1361, 2008.

[3] B. R. Mahafza, *Radar Systems Analysis and Design Using Matlab*, Boca Raton, FL: Capman & Hall/CRC, 2000.

[4] D. K. Barton, *Radar System Analysis and Modeling*, Boston: Artech House, 2005.

[5] N. A. Goodman, "Optimum and decentralized detection for multistatic airborne radar," *IEEE Transactions on Aerospace and Electronic Systems*, vol. 43, no. 2, pp. 806-813, 2007.

[6] Z. A. Hussein, B. Holt, K. C. McDonald, R. Jordan, J. Huang, Y. Kuga, A. Ishimaru, S. Jaruwatanadilok, S. Gogineni., and T. Akins "High resolution VHF interferometer SAR sensor and technique for sea ice thickness measurement," *IGARSS*, Denver, CO, 2006.

[7] S. Jaruwatanadilok, A. Ishimaru, and Y. Kuga, "Snow thickness estimation using correlation function," *IGARSS*, Anchorage, AK, USA, 2006.

[8] L. Tsang, J. A. Kong, *Scattering of Electromagnetic Waves: Advanced Topics*, New York: John Wiley & Sons, 2001.

[9] C. T. C. Le, Y. Kuga, and A. Ishimaru, "Angular correlation function based on the second-order Kirchhoff approximation and comparison with experiment," *Journal of the Optical Society of America A*, vol. 13, no. 5, pp.1057-67, 1996.

[10] C. A. Balanis, *Advanced Engineering Electromagnetics*, New York: John Wiley & Sons, 1989.

[11] A. A. Nilsson and T. H. Glisson, "On the Derivation and numerical evaluation of the Weibull-Rician distribution," *IEEE Transactions on Aerospace and Electronic Systems*, vol. AES-16, no. 6, pp. 864-867, 1980.

[12] R. Dusseaux and R. de Oliveira, "Effect of the illumination length on the statistical distribution of the field scattered from one-dimensional random rough surfaces: analytical formulae derived from the small perturbation method," *Wave in Random and Complex Media*, vol. 17, no. 3, pp. 305-320, 2007.

[13] J. Salo, H. M. El-Sallabi, and P. Vainikainen, "The distribution of the product of independent Rayleigh random variables," *IEEE Transactions on Antennas and Propagation*, vol. 54, no. 2, pp. 639-643, 2006.

[14] V. Erceg, S. J. Fortue, J. Ling, A. J. Rustako, and R. A. Valenzula, "Comparisons of a computer-based propagation prediction tool with experimental data collected in urban microcellular environments," *IEEE Journal on Selected Areas in Communications*, vol. 15, no.4, pp. 677-684, 1997.

[15] A. Ishimaru, *Wave Propagation and Scattering in Random Media*, New York: Academic, 1978.

[16] M. Abramowitz and I. A. Stegun, *Handbook of Mathematical Functions: with Formulas, Graphs, and Mathematical Tables*, New York: Dover, 1970.